

## Spectral Models of the Type Ic SN 1994I in M51

E. Baron, David Branch

*Dept. of Physics and Astronomy, University of Oklahoma, 440 W. Brooks, Rm 131, Norman, OK 73019-0225*

[baron@mail.nhn.ou.edu](mailto:baron@mail.nhn.ou.edu), [branch@mail.nhn.ou.edu](mailto:branch@mail.nhn.ou.edu)

Peter H. Hauschildt

*Dept. of Physics and Astronomy & Center for Simulational Physics, University of Georgia, Athens, GA 30602-2451*

[yeti@hal.physast.uga.edu](mailto:yeti@hal.physast.uga.edu)

Alexei V. Filippenko

*Dept. of Astronomy, University of California, Berkeley, CA 94720-3411*

[alex@astro.berkeley.edu](mailto:alex@astro.berkeley.edu)

and

R. P. Kirshner

*CfA, 60 Garden St., Cambridge, MA 02138*

[kirshner@cfa.harvard.edu](mailto:kirshner@cfa.harvard.edu)

### ABSTRACT

We present detailed non-local thermodynamic equilibrium (NLTE) synthetic spectra for comparison with a time series of observed optical spectra of the Type Ic supernova 1994I which occurred in M51. With the exceptions of Si I and S I, we treat the important species in the formation of the spectrum in full NLTE. We present results for both a hydrodynamic model that has been fit to the light curve and for an illustrative custom crafted model that is more massive. Both models give reasonable fits to the overall observed spectra; however, neither is able to reproduce all the observed features. Some conspicuous observed features are absent and some predicted features are unobserved. No model that we have explored is able to satisfactorily reproduce the observed infrared feature near  $1 \mu m$  on April 15, 1994 (+7d), which has been attributed to the triplet He I  $\lambda 10830$  transition. The low-mass hydrodynamic model produces an infrared feature with a blend of He I, C I, O I, and Si I-II lines, but it predicts a strong unobserved absorption feature near 6100 Å due to Fe III, and the observed feature just blueward of 6000 Å

most likely due to Na D is not reproduced. The more massive model does a better job of reproducing the observed infrared lineshape, but also predicts the unobserved feature near 6100 Å. The early-time spectrum of the low-mass model is far too blue; thus, a more massive model may be slightly favored. Since the predicted infrared feature is produced by a blend of so many elements and there is no overwhelming evidence for other helium features such as  $\lambda 5876$ , it may be premature to conclude that SNe Ic unambiguously contain helium. Thus, we conclude that pure C+O cores are still viable progenitors for SNe Ic.

*Subject headings:* radiative transfer — supernovae: individual (SN 1994I) — supernovae: general

## 1. Introduction

Type I supernovae are classified on the basis of their spectra. SNe Ia have strong Si II  $\lambda 6355$  lines in their spectra where the absorption minimum is typically shifted to around 6100 Å near maximum light, April 8, 1994 (Richmond et al. 1996), and their late-time spectra are dominated by iron peak elements. SNe Ib have weak or absent Si II lines, but strong optical He I  $\lambda 5876$  and  $\lambda 6678$  at maximum light, with late-time spectra dominated by lines of [O I] and [Ca II]. SNe Ic appear very similar to SNe Ib at late times, but they lack the strong He I lines at early times.

Supernova 1994I, which occurred in the nearby galaxy M51, is undoubtedly the best studied Type Ic supernova to date (Filippenko et al. 1995; Baron et al. 1996; Wheeler et al. 1995; Iwamoto et al. 1994; Nomoto et al. 1994; Woosley & Eastman 1997; Richmond et al. 1996; Woosley et al. 1993; Clocchiatti et al. 1996; Millard et al. 1999). As originally classified (Harkness & Wheeler 1990; Wheeler & Harkness 1990), SNe Ic were thought to show a complete absence of He I lines. However, Filippenko et al. (1995) identified He I  $\lambda 10830$  in the spectrum of SN 1994I and Clocchiatti et al. (1996) have inferred the presence of weak He I  $\lambda 5876$  and  $\lambda 6678$  lines in SN 1994I as well as in SN Ic 1987M.

The apparent absence of helium in the spectra of the first few observed SNe Ic led to the inference that the progenitor star was likely to be a bare (or nearly bare) C+O core of a massive star, which explodes due to the collapse of the iron core to form a neutron star (Wheeler & Harkness 1990; Harkness & Wheeler 1990). The helium envelope of the massive star could be stripped from the star either through extensive mass loss in a Wolf-Rayet phase, via interaction with a binary companion, or a combination of the two (Wheeler & Harkness 1990; Harkness & Wheeler 1990; Filippenko et al. 1990; Podsiadlowski et al. 1992; Woosley et al. 1993; Nomoto et al. 1994). On the basis of the rate of decline of the light curve, Nomoto and collaborators suggested that the difference between SNe Ib and SNe Ic was due to the mass and degree of mixing, with SNe Ic being both less massive and more mixed (Nomoto et al. 1990, 1991; Yamaoka & Nomoto 1991; Hachisu et al. 1991; Jeffery et al. 1991; Branch et al. 1991). Since helium is the diagnostic for SNe Ib, it

has been suggested that SNe Ib should in fact be the more thoroughly mixed ones (Baron 1992; Woosley & Eastman 1997).

## 2. Model Construction

Hydrodynamic models of SN 1994I have been constructed to fit the light curve for single star progenitors (Woosley et al. 1993; Woosley & Eastman 1997) and for binary progenitors (Iwamoto et al. 1994). We use the CO21 model of Iwamoto et al. (1994) (total ejected mass =  $0.9 M_{\odot}$ , total deposited energy =  $1 \times 10^{51}$  ergs, and a parameterized model constructed by us to represent the more massive core favored by Woosley and collaborators (Woosley et al. 1993; Woosley & Eastman 1997). The parameterized model is constructed by specifying a density profile, taken to be  $\rho \propto r^{-N}$ , with  $N = 8$ , a model temperature  $T_{\text{model}} = 6800$  K, the reference radius  $R_0$ , which is the radius where the continuum optical depth in extinction at 5000 Å ( $\tau_{\text{std}}$ ) is unity, the expansion velocity,  $v_0 = 6000$  km s $^{-1}$ , at the reference radius, which is determined by fitting the width and position of the observed spectral features (and using homologous expansion,  $R_0 = v_0 t$  where  $t$  is the time since explosion and we have used an explosion date of Mar 30 in these calculations, 9 days before B max), and finally the elemental abundances. The total ejected mass of the model is  $2.4 M_{\odot}$ , with a kinetic energy of  $1.3 \times 10^{51}$  ergs. The total nickel mass is about  $0.1 M_{\odot}$ ; however, since we use only a local deposition function, no strong physical significance should be attached to this value and it is only indicative (this is not the case for the hydrodynamical models where the deposition function is calculated accurately). Setting the elemental abundances leads in principle to 1950 free parameters, since we include 39 elements and we must specify the relative number fraction of each of these elements in each of the 50 radial zones used in the calculations. In order to minimize the number of abundance parameters we follow our previous work (Baron et al. 1996) and begin with a solar abundance (Anders & Grevesse 1989) and then “burn” all the hydrogen to helium. Next we “burn” some helium to carbon and oxygen with a final number ratio He/O, and a production ratio by number of carbon to oxygen (C/O). Finally we allow metals heavier than oxygen to be scaled by a factor  $Z$  (taken equal to the solar value in the model we present here, although we have studied the effects of varying the model content by up to 3 times the solar value, we find our results to be insensitive to the metallicity in this range). While in our previous models of SN 1994I (Baron et al. 1996) the composition was uniform throughout the model, in these calculations that assumption is relaxed. The hydrodynamic models are fully non-uniform in composition. In the parameterized models we consider only 2 regions which consist of differing composition; a primarily helium composition of total mass  $M = 0.06 M_{\odot}$  (for the model presented here He/O = 10), the remaining portion was primarily C/O composition (for the model presented here He/O = 1, so helium was somewhat mixed throughout the model). A final parameter of the model was the total mass of the ejecta. We note that while  $T_{\text{model}}$  is a parameter used to fit the spectral shape, if the abundances, velocities, and density structure are in significantly error no choice of  $T_{\text{model}}$  will lead to a reasonable fit to the overall shape of the spectrum.

While we present here the results of our single “best” model we base our conclusions on our total parameter study which for April 15 alone consisted of 33 different compositions, 5 different total masses and a range of deposition functions (or degree of mixing of Ni) that spanned 4 orders of magnitude. The parameter study included allowing for 3 differing compositions (a nearly pure helium layer, a mixed C/O + He layer, and a nearly pure C/O layer).

Our choice of a local deposition function implies that the nickel is distributed throughout the atmosphere with a constant mass fraction and the non-thermal ionization rates are then calculated assuming that all of the gamma-ray energy instantaneously produced is deposited locally. Of course radioactive decay of the nickel is accounted for. Although this is a somewhat crude approximation, it is expedient and by varying the assumed nickel mass fraction we can simply study the effects of mixing. At high optical depths where the matter is in LTE, the assumed deposition function is irrelevant (our results show that we recover the LTE populations exactly) and thus we really can probe the effects of nickel mixing in the line forming region with this simple approximation.

For the hydrodynamical models our procedure was the same as described in Nugent et al. (1997). The results from the hydrodynamical calculations were expanded homologously, radioactive decay was included when adjusting the compositions, and the gamma-ray deposition function was calculated assuming pure absorptive gamma-ray opacity and local deposition of positrons. Although Milne et al. (1999) find that local deposition of positrons likely overestimates the energy deposition of positrons at late times in Type Ia supernovae, this assumption should have negligible effects on the early times we explore here.

Figures 1 and 2 present the most important species in the two models (CO21 and our more massive parameterized model for the April 15 [+7d] epoch) as a function of velocity. Figure 3 displays the velocity as a function of  $\tau_{\text{std}}$  (the total continuum extinction optical depth at 5000 Å) in order to aid in the interpretation of the abundance figures. These ions (O I-II, He I-II, C I-II, Si II-III, Mg II), are expected and support the line identifications herein and in Millard et al. (1999).

The synthetic spectra predicted by the constructed models were then computed using the generalized stellar atmosphere code **PHOENIX** (cf. Hauschildt & Baron 1999, and references therein). Table 1 lists the ions and number of levels/transitions that we treat in full NLTE in these calculations. **PHOENIX** is capable of treating a larger number of species in NLTE, but we have chosen the most important species for these conditions. Even with this subset of NLTE species each model calculation takes about 1 day using 5 thin-2 nodes of an IBM SP2 parallel supercomputer.

### 3. Results

Figure 4 displays our synthetic spectrum for the CO21 model of Iwamoto et al. (1994), compared to the spectrum taken at Lick Observatory on April 15, 1994 (+7d). The observed spectrum has been dereddened using the reddening law of Cardelli et al. (1989) and assuming  $E(B-V) = 0.45$  mag. Since the supernova shows very strong interstellar Na absorption lines and occurred in

a dust lane in M51, the reddening is very uncertain. Values of  $E(B-V)$  in the range  $0.30 - 0.45$  mag (Baron et al. 1996; Richmond et al. 1996) are reasonable and altering the reddening in this range will not greatly affect our results. Figure 5 displays our best fit with our massive model. Neither the CO21 model nor the massive model are able to reproduce all of the observed features. In particular, neither of the models predicts the strong observed absorption feature near  $5800 \text{ \AA}$ , which is likely produced by the Na D lines (Millard et al. 1999).

The CO21 model does a reasonable job at fitting the overall lineshape of the observed infrared feature, which it does with a blend of He I and C I  $\lambda 10695$  (and other C I) as well as O I and Si I-II lines. However, the CO21 model also produces strong, unobserved optical absorption features near  $5000 \text{ \AA}$ , mostly due to Fe III. The CO21 model also does a rather poor job reproducing the O I  $\lambda 7773$  feature and the Ca II IR triplet.

The massive model has less of a problem with the strong absorption near  $5000 \text{ \AA}$  and even begins to reproduce the observed Fe II features in that region of the spectrum, indicating that the ionization states of the iron-peak elements is better reproduced in this model. The O I  $\lambda 7773$  feature is even weaker in this model than in the CO21 model, but the Ca II IR triplet is better reproduced. Both models do poorly at reproducing the flat bottomed absorption feature near  $6250 \text{ \AA}$ , which is produced either by the Si II  $\lambda 6355$  line or by the C II  $\lambda 6580$  line in a detached shell as proposed by Millard et al. (1999). We discuss the identity of the features in detail in § 4.

Figures 6–8 display the time history of the CO21 model. In general the overall shape of the spectra is reasonably well reproduced by the model, but the features themselves are not. Figures 6 shows that the model calculation is too blue at early times. This is almost certainly due to the very low-mass in the ejecta and may also indicate that more Fe is required in the models. Therefore the need for a somewhat more massive model is indicated both by the early spectra and by the April 15 (+7d) spectrum.

#### 4. Discussion

Our models show that overall, an ejecta mass near  $2.4 M_{\odot}$ , with a mostly C+O+He composition, leads to reasonably good agreement with the observed spectra near maximum light. Nevertheless, it is useful to examine the deficiencies of the hydrodynamic model and to explore what the possible line identifications in the observed spectra are by using sophisticated models. This is especially important once one realizes that in detailed calculations the features that are usually identified as due to a single line are in reality produced by blends of many different features that form in many places in the supernova “atmosphere.” Figure 9 displays the spectra produced using the structure of Figure 4, but with *all LTE line opacities set to zero* and only the indicated NLTE line opacities included; all continuum opacities are included in all the calculations. Examining the spectrum with *only* continuum opacities we see that the “emission” feature near  $3800 \text{ \AA}$  is in fact the result of a (C II) continuum edge. This fact should lead to caution in identifying features (and

deriving velocity information) based solely on wavelength coincidences. The Fe II and Co II spectra lead to features that are recognizable and unremarkable although they appear to be too weak in the synthetic spectrum. The Fe III and Co III lines are too strong and lead to the unobserved features near 5000 and 6100 Å, indicating that the iron-peak elements are over-ionized. While the 6100 Å feature is weak in this figure, we believe it is masking the observed Na D feature. This is a clear sign that the mass of the CO21 model is too low, since if the iron-peak elements were at higher density they would be more likely to recombine. The temperature structure of the atmosphere, (and therefore our value of the total bolometric luminosity), is reasonably well determined since it is clearly required to reproduce the overall shape of the spectrum. The He I spectrum is interesting, in that it produces a relatively weak He I  $\lambda$ 5876 line and a He I  $\lambda$ 10830 feature that is essentially in emission. In the full spectrum (Figure 4) there is no evidence of the He I  $\lambda$ 5876 feature and clearly the predicted feature due to He I  $\lambda$ 10830 is too weak to have fully produced the observed infrared feature; therefore in our models this feature must be produced by additional contributions from C I, O I, and Si I–II (Si I is treated in LTE in our calculations). Swartz et al. (1993) find that whenever He I  $\lambda$ 10830 is present, so too are He I  $\lambda$ 5876 and He I  $\lambda$ 6678. While this result lends credence to our suggestion that the IR feature is in fact produced by alternate species, rather than by helium, we don't find the He I  $\lambda$ 10830 to be as pronounced as they do in their calculations, which could be caused by the fact that we are examining different epochs or that we treat more species and complex blending effects diminish the strength of the He I  $\lambda$ 10830 line. The spectrum produced by Si II in Figure 9 is also notable in that it predicts a feature from the Si II  $\lambda$ 6355 line that is not noticeable in the full synthetic spectrum. Since the infrared feature is produced to some extent in our calculations by Si I, it is clearly important to include this species in NLTE in future work. Millard et al. (1999) have shown that in parameterized calculations it is not possible to determine whether the feature ascribed to He I  $\lambda$ 10830 is due to a blend of He I and C I or to a blend of Si I lines. The fact that the infrared feature is produced by a blend of a number of different species in our calculations should lead to caution when making line identifications based solely on wavelength, particularly when there is only a single feature from an identified species.

Since the excited states of He I lie so high above the ground state, a good predictor for the strength of the He I lines is the abundance of He II. The fact that He II is prevalent in our parameterized model (see Figure 2), and somewhat less prevalent in the CO21 model, probably leads to the more massive parameterized model's better reproduction of the observed lineshapes and lends some support for the identification of the line as due to helium. This support should be tempered by the realization that our treatment of gamma-ray deposition in the massive model is parameterized and not based on direct hydrodynamical calculations. However, we have varied the value of the deposition function by 4 orders of magnitude which mimics a huge range in mixing (probably a larger range than is physically reasonable). Additionally, the fact that in the CO21 model the observed infrared feature is produced by a blend of other lines should lead to caution in the identification of helium in SN 1994I in particular, and SNe Ic in general. Although Clocchiatti et al. (1996) argue that the absence of a redward shift in the Na D feature is evidence for He I  $\lambda$ 5876 in SN 1994I, there is another feature of the same strength just blueward that is unidentified

in their spectra; thus, while indicative, these features are not conclusive evidence for the presence of He I. A hydrodynamical model that does a better job of reproducing the spectrum is needed. Such a model would likely be more massive than CO21, have the iron-peak elements concentrated in the first ionization stage, and have more Si II at low velocity. Also, since the Na D line is not well reproduced in any of our models, we suspect that the gamma-ray deposition is incorrectly ionizing the sodium.

Fassia et al. (1998) find that in order to fit the observed infrared feature (which they assume to be due to He I  $\lambda 10830$ ) in the Type II SN 1995V, they need both dredge-up of  $^{56}\text{Ni}$  into the hydrogen envelope as well as clumping of helium within the hydrogen envelope. Given the fact that their models fail to fit the O I  $\lambda 7773$  line and that blending with O I and Si I-II lines may be important in SNe II as well as SNe Ib/c, it seems prudent to view any conclusions based solely on the apparent presence of He I  $\lambda 10830$  in SNe with caution. Clearly detailed synthetic spectral models of high-quality hydrodynamic simulations is the best way to draw firm conclusions about the structure of the supernova ejecta.

We note that since we have not calculated the spectra produced by the model of Woosley and collaborators (Woosley et al. 1993; Woosley & Eastman 1997), our results certainly are compatible with that model and it should still be considered a viable candidate. Our most important result is, however, that the IR feature that has been attributed to helium, is *not* a clear indicator of the presence of helium, since it can be produced both by a blend of Si I lines (Millard et al. 1999), or at the very least consists of a blend of helium and carbon. All the models that we have explored where the feature was produced explicitly by helium showed strong optical helium features in agreement with the results of Millard et al. (1999). Finally, we note that future explosion models should focus on more massive progenitors and should consider models with and without helium in order to determine the identity of the observed IR-feature.

We thank Peter Höflich and Ken Nomoto for helpful discussions and for providing us with the CO21 model. This work was supported in part by NSF grants AST-9417213, AST-9417242, AST-9731450, and AST-9417102; NASA grant NAG5-3505; an IBM SUR grant to the University of Oklahoma; and NSF grant AST-9720704, NASA ATP grant NAG 5-3018, and LTSA grant NAG 5-3619 to the University of Georgia. Some of the calculations presented in this paper were performed at the San Diego Supercomputer Center (SDSC), supported by the NSF, and at the National Energy Research Supercomputer Center (NERSC), supported by the U.S. DOE. We thank both of these institutions for a generous allocation of computer time.

## REFERENCES

Anders, E. & Grevesse, N. 1989, *Geochim. Cosmochim. Acta*, 53, 197

Baron, E. 1992, *MNRAS*, 255, 267

Baron, E., Hauschildt, P. H., Branch, D., Kirshner, R. P., & Filippenko, A. V. 1996, MNRAS, 279, 779

Branch, D., Nomoto, K., & Filippenko, A. V. 1991, Comments on Astrophysics, 15, 221

Cardelli, J. A., Clayton, G. C., & Mathis, J. S. 1989, ApJ, 345, 245

Clocchiatti, A., Wheeler, J. C., Brotherton, M., Cochran, A., Wills, D., Barker, E., & Turatto, M. 1996, ApJ, 462, 462

Fassia, A., Meikle, W. P. S., Geballe, T., Walton, N., Pollaco, D., Rutten, R., & Tinney, C. 1998, MNRAS, 299, 150

Filippenko, A. V., Porter, A. C., & Sargent, W. L. W. 1990, AJ, 100, 1575

Filippenko, A. V. et al. 1995, ApJ, 450, L11

Hachisu, I., Matsuda, T., Nomoto, K., & Shigeyama, T. 1991, ApJ, 368, L27

Harkness, R. & Wheeler, J. C. 1990, in Supernovae, ed. A. Petschek (New York: Springer-Verlag), 1

Hauschildt, P. H. & Baron, E. 1999, J. Comp. Applied Math., in press

Iwamoto, K., Nomoto, K., Höflich, P., Yamaoka, H., Kumagai, S., & Shigeyama, T. 1994, ApJ, 437, L115

Jeffery, D., Branch, D., Filippenko, A. V., & Nomoto, K. 1991, ApJ, 377, L89

Millard, J., Branch, D., Baron, E., Hatano, K., Fisher, A., Filippenko, A. V., Kirshner, R. P., Challis, P. M., Fransson, C., Panagia, N., Phillips, M. M., Sonneborn, G., Suntzeff, N. B., Wagoner, R. V., & Wheeler, J. C. 1999, ApJ, in press

Milne, P., The, L.-S., & Leising, M. 1999, ApJ, in press

Nomoto, K., Filippenko, A. V., & Shigeyama, T. 1990, A&A, 240, L1

Nomoto, K., Shigeyama, T., Kumagai, S., Hachisu, I., & Matsuda, T. 1991, in Proceedings of the ESO/EPIC Workshop on SN 1987A and other Supernovae, ed. I. J. Danziger & K. Kjär (Munich: ESO), 173

Nomoto, K., Yamaoka, H., Pols, O. R., van den Heuvel, E. P. J., Iwamoto, K., & Shigeyama, T. 1994, Nature, 371, 227

Nugent, P., Baron, E., Branch, D., Fisher, A., & Hauschildt, P. 1997, ApJ, 485, 812

Podsiadlowski, P., Joss, P. C., & Hsu, J. J. L. 1992, ApJ, 391, 245

Richmond, M. W. et al. 1996, AJ, 111, 327

Schmidt, B. & Kirshner, R. P. 1994, private communication

Swartz, D. A., Filippenko, A. V., Nomoto, K., & Wheeler, J. C. 1993, *ApJ*, 411, 313

Wheeler, J. C. & Harkness, R. 1990, *Repts. Prog. Phys.*, 53, 1467

Wheeler, J. C., Harkness, R. P., Clocchiatti, A., Benetti, S., Brotherton, M. S., DePoy, D. L., & Elias, J. 1995, *ApJ*, 436, L135

Woosley, S. E. & Eastman, R. G. 1997, in *Thermonuclear Supernovae*, ed. P. Ruiz-Lapuente, R. Canal, & J. Isern (Dordrecht: Kluwer), 821

Woosley, S. E., Langer, N., & Weaver, T. A. 1993, *ApJ*, 411, 823

Yamaoka, H. & Nomoto, K. 1991, in *Proceedings of the ESO/EPIC Workshop on SN 1987A and other Supernovae*, ed. I. J. Danziger & K. Kjär (Munich: ESO), 193

Table 1. NLTE Species

Element	Ionization Stage		
	I	II	III
H	15/105	...	...
He	11/14	...	...
C	228/1387	85/336	79/365
O	36/66	171/1304	...
Ne	26/37	...	...
Na	3/2	...	...
Mg	...	18/37	...
Si	...	93/436	155/1027
S	...	84/444	41/170
Ca	...	87/455	...
Fe	494/6903	617/13675	566/9721

Note. — The species and number of levels/transitions treated in non-LTE by PHOENIX in these calculations.

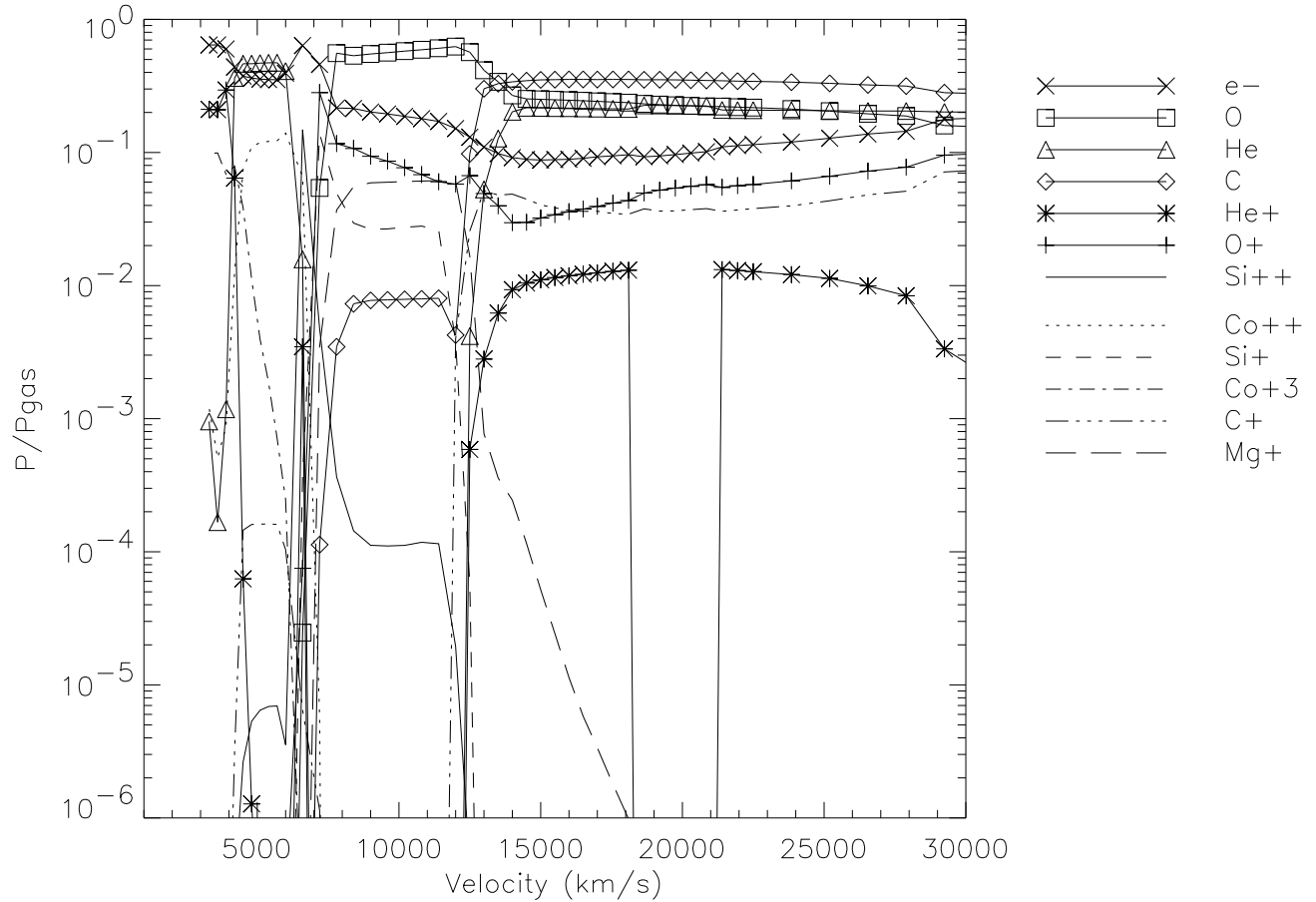


Fig. 1.— The partial pressures of the most prevalent species in the CO21 model as a function of velocity for the April 15 (+7d) epoch. (The synthetic spectrum produced by this model is shown in Figure 4.)

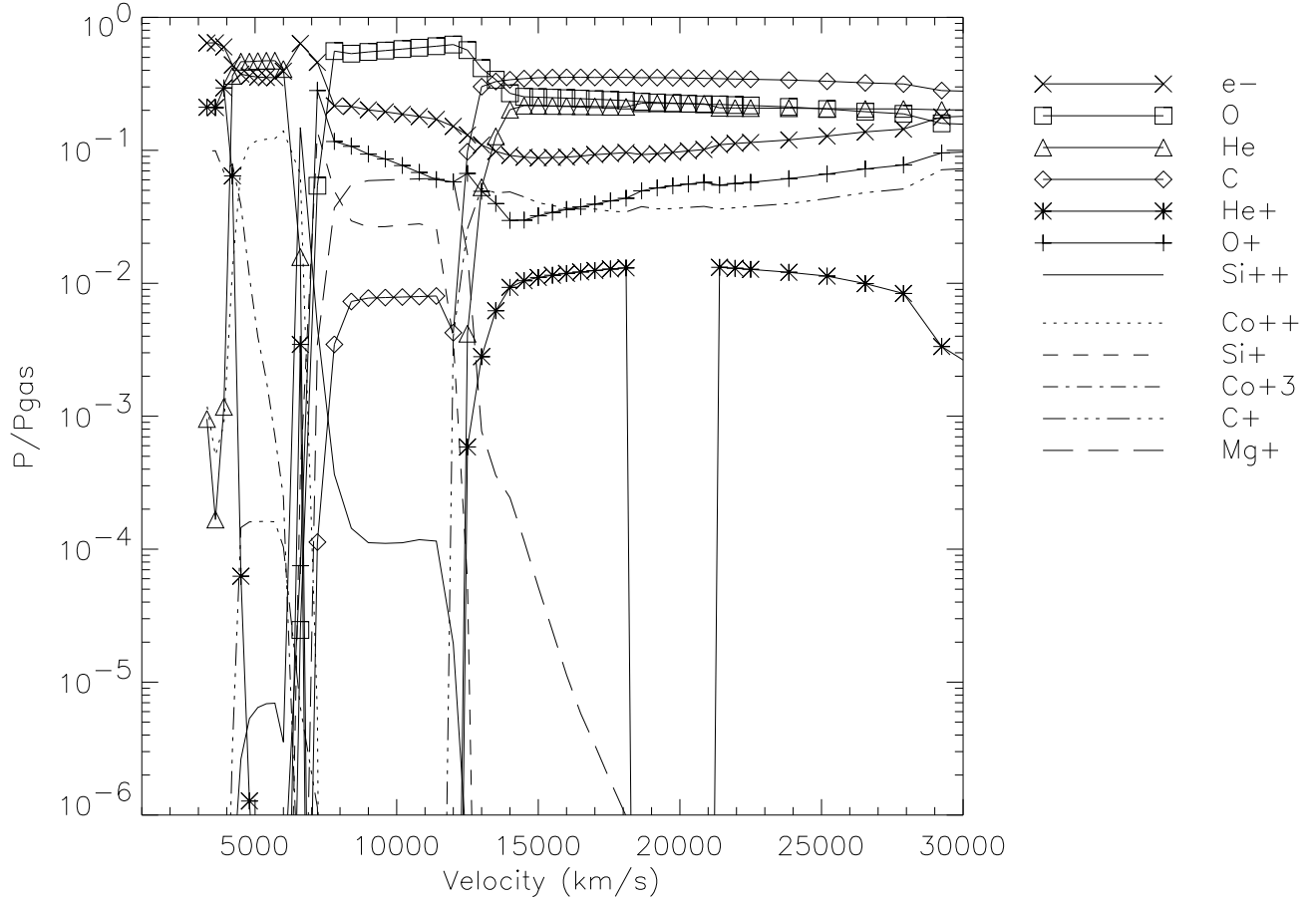


Fig. 2.— The partial pressures of the most prevalent species as a function of velocity in the parameterized more massive model for the April 15 (+7d) epoch. (The synthetic spectrum produced by this model is shown in Figure 5.)

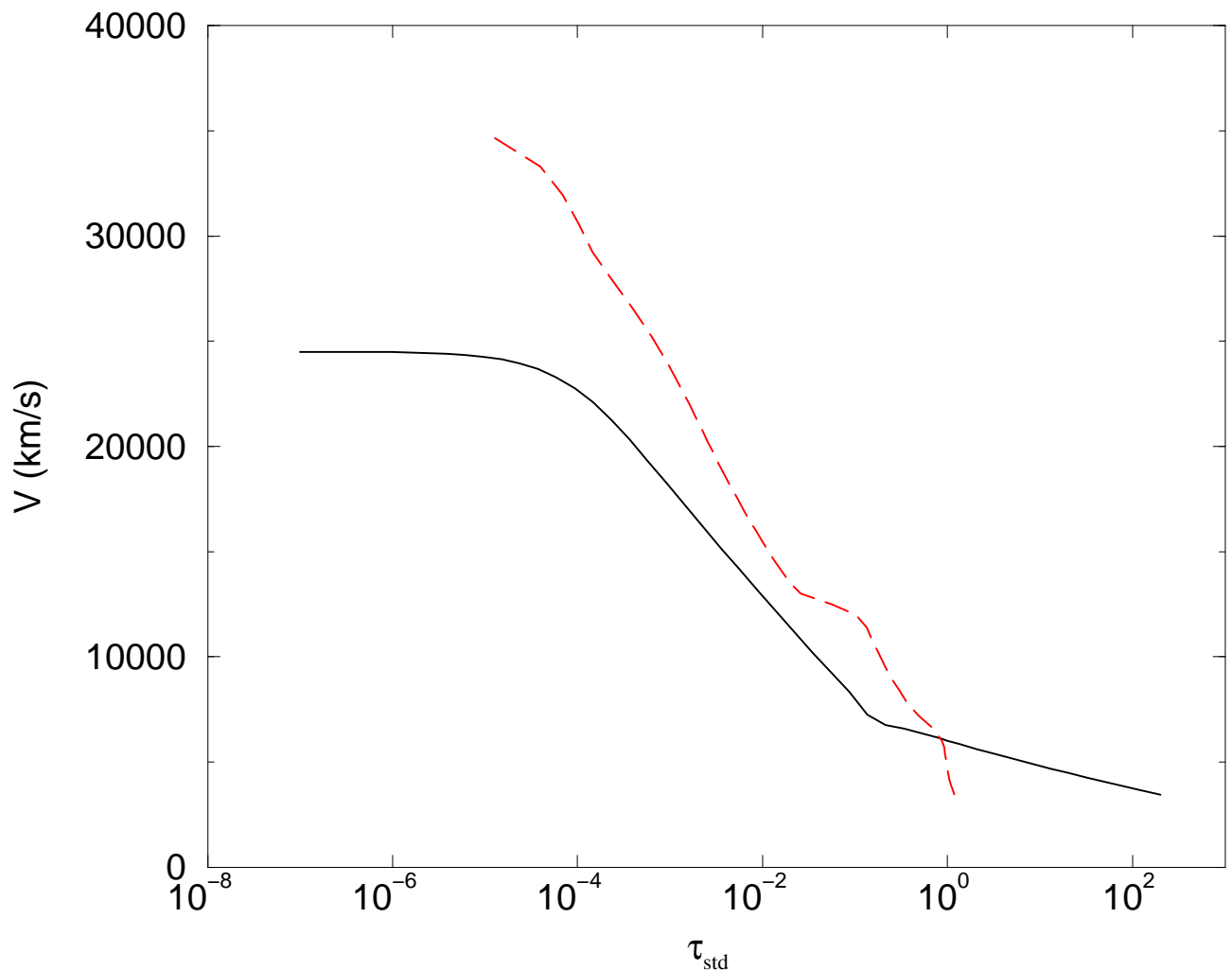


Fig. 3.— The velocity profiles of the two models in Figures 1 (dashed line) and 2 (solid line).  $\tau_{\text{std}}$  is the total continuum optical depth at 5000 Angstroms.

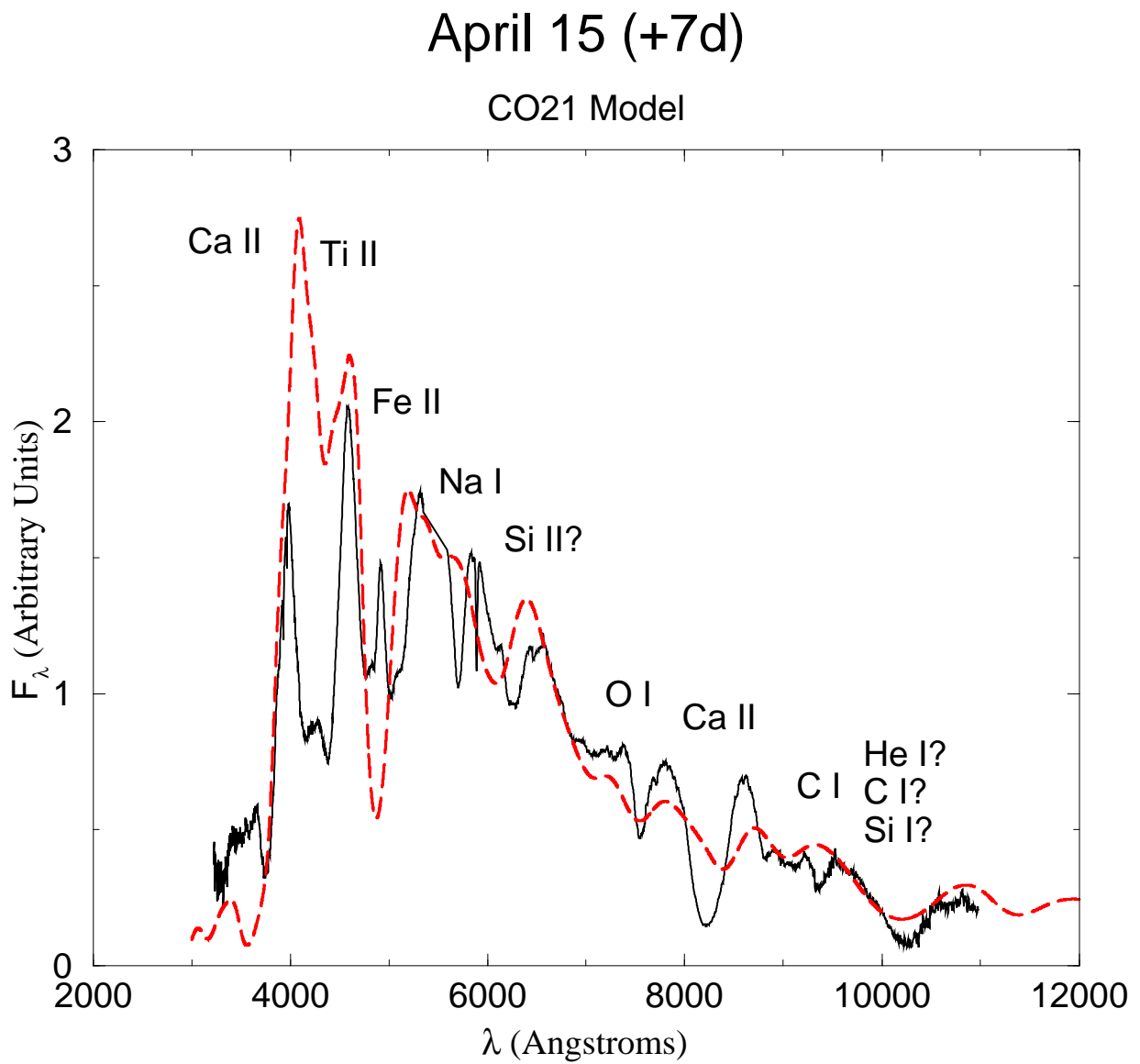


Fig. 4.— The synthetic spectrum of the Iwamoto et al. (1994) model (dashed curve) is compared to the spectrum taken at Lick Observatory on April 15, 1994 (+7d) (Filippenko et al. 1995). The line identifications are the combined results of this work and that of Millard et al. (1999).

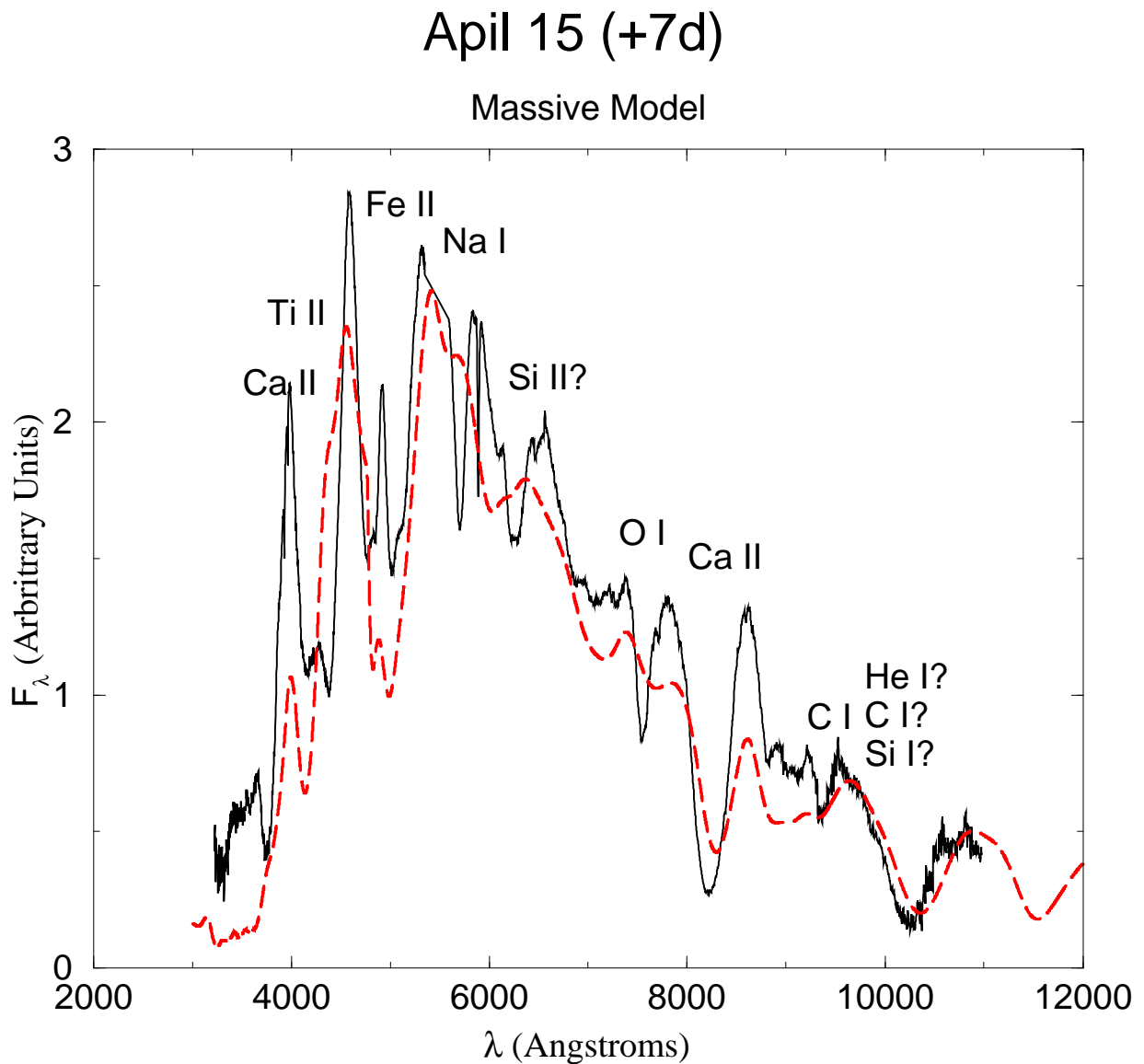


Fig. 5.— The synthetic spectrum of our massive star model (dashed curve) is compared to the spectrum taken at Lick Observatory on April 15, 1994 (+7d) (Filippenko et al. 1995).

April 4 (–4d)

CO21 Model

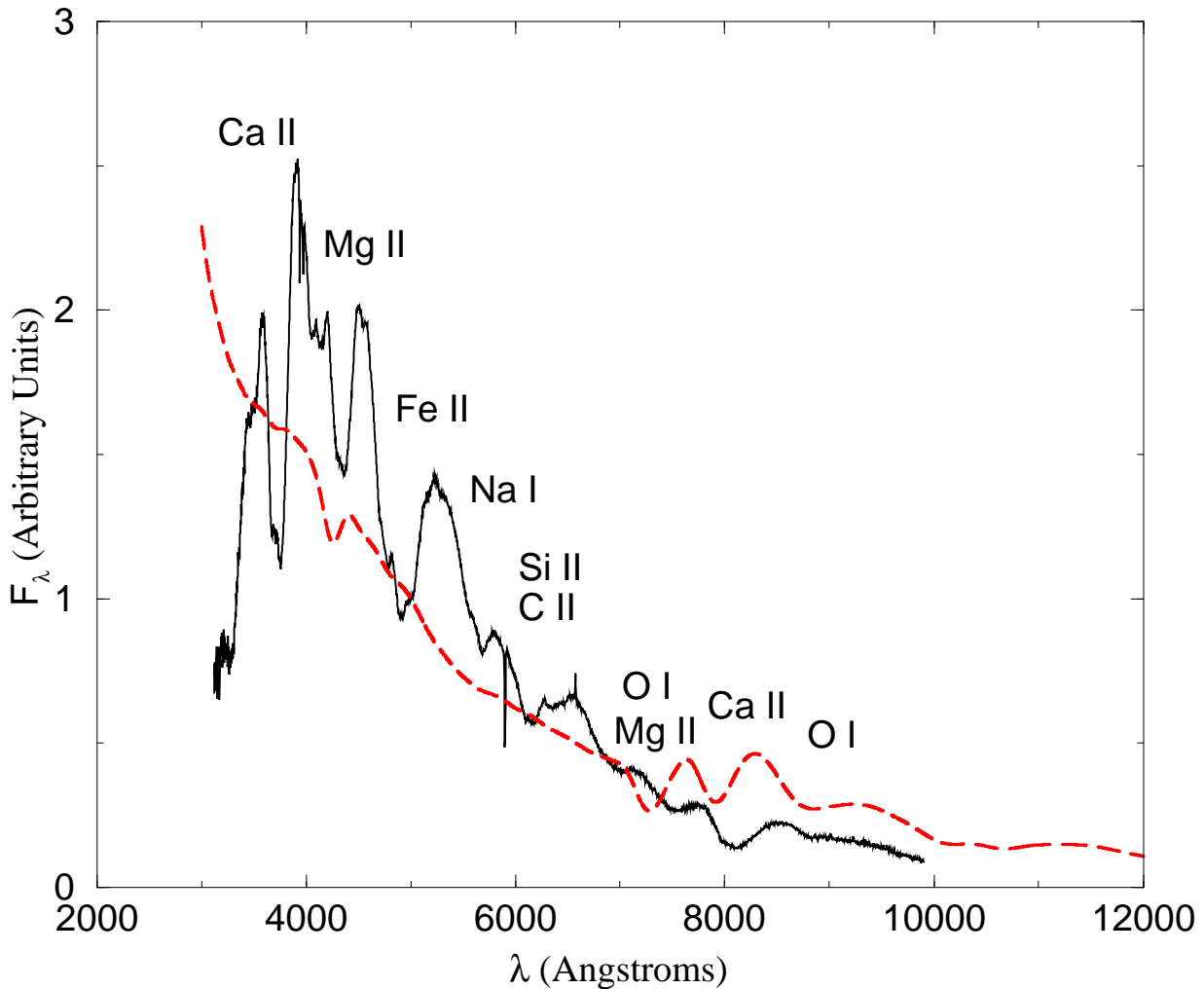


Fig. 6.— The synthetic spectrum of the Iwamoto et al. (1994) model (dashed curve) is compared to the spectrum taken at Lick Observatory on April 4, 1994 (–4d) (Filippenko et al. 1995).

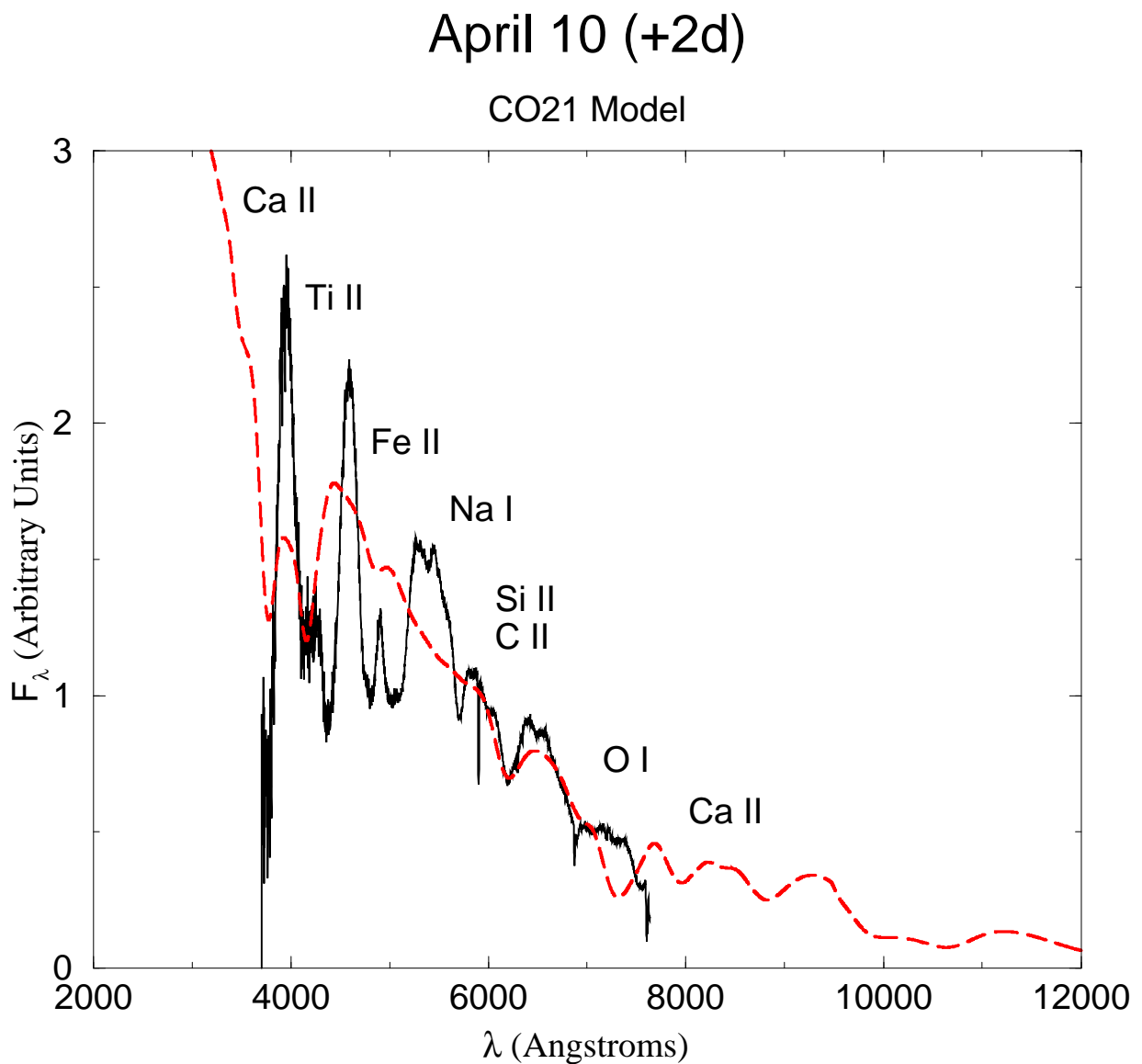


Fig. 7.— The synthetic spectrum of the Iwamoto et al. (1994) model (dashed curve) is compared to the spectrum taken at the MMT on April 10, 1994 (+2d) (Schmidt & Kirshner 1994).

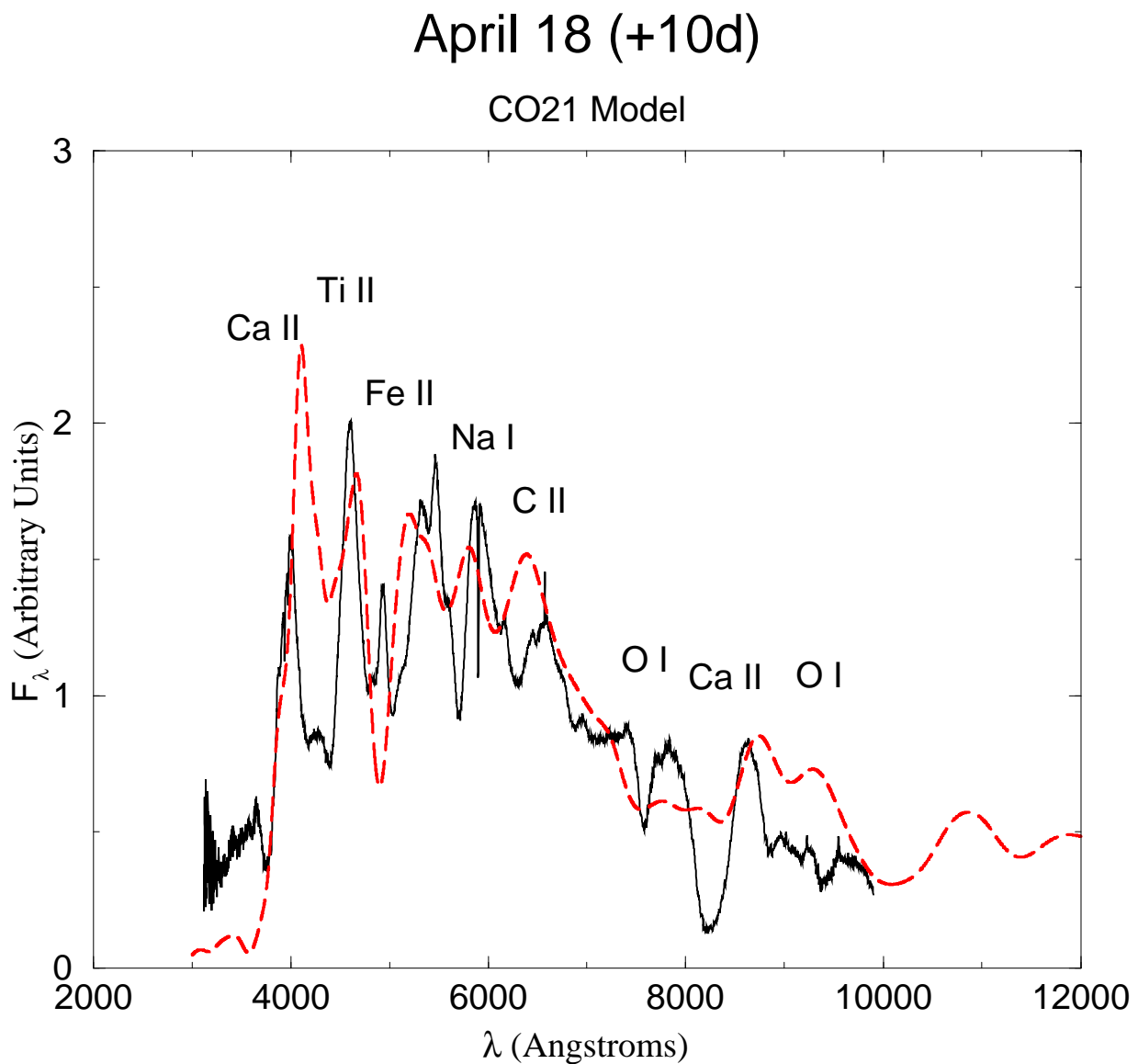


Fig. 8.— The synthetic spectrum of the Iwamoto et al. (1994) model (dashed curve) is compared to the spectrum taken at Lick Observatory on April 18, 1994 (+10d) (Filippenko et al. 1995).

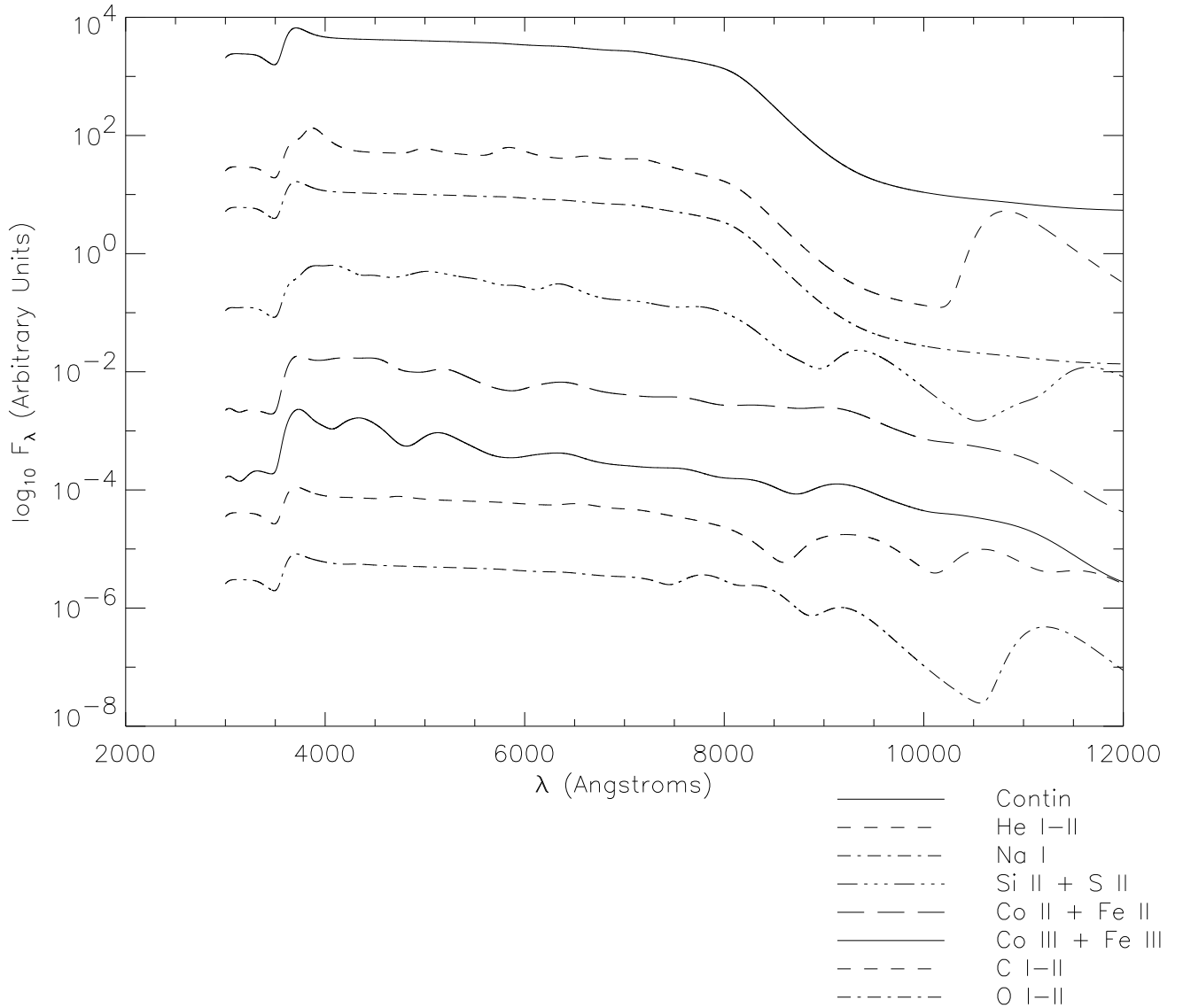


Fig. 9.— The model spectra for the identical conditions as displayed in Figure 4, but with only NLTE line opacity included; all LTE line opacity has been set to zero. The legend indicates which particular NLTE lines are included in the calculations.